

## CONTROLLING MECHANISMS FOR MOLYBDENUM ISOTOPE FRACTIONATION IN PORPHYRY DEPOSITS: THE QULONG EXAMPLE

Yang Li,<sup>1,†</sup> Alex J. McCoy-West,<sup>2,3</sup> Shuang Zhang,<sup>4</sup> David Selby,<sup>3,5</sup> Kevin W. Burton,<sup>3</sup> and Kate Horan<sup>3</sup>

<sup>1</sup>*State Key Laboratory of Lithospheric Evolution, Institute of Geology and Geophysics,  
Chinese Academy of Sciences, Beijing 10029, China*

<sup>2</sup>*School of Earth, Atmosphere and Environment, Monash University, Melbourne, Victoria 3800, Australia*

<sup>3</sup>*Department of Earth Sciences, Durham University, Durham, DH1 3LE, UK*

<sup>4</sup>*Department of Geology and Geophysics, Yale University, New Haven, Connecticut 06511, USA*

<sup>5</sup>*State Key Laboratory of Geological Processes and Mineral Resources, School of Earth Resources,  
China University of Geoscience, Wuhan, Hubei 430074, China*

### Abstract

Molybdenite-bearing porphyry deposits are the predominant supplier of molybdenum to industrialized society and one of the main hosts of Mo in the upper continental crust. The Mo isotope compositions ( $\delta^{98/95}\text{Mo}$ , normalized to NIST3134 equals 0‰) of molybdenite show considerable variation (–1.62 to +2.27‰), but the factors controlling this variability remain poorly constrained. This information is critical for underpinning genetic models of porphyry deposits, understanding elemental cycling, and utilizing the  $\delta^{98/95}\text{Mo}$  of marine sediments as a paleoredox proxy. Using the well-characterized Qulong porphyry Cu–Mo deposit (Tibet) as an example, here we discuss how rapid cooling, facilitated by mixing hot magmatic fluid with cold meteoric water, can be a controlling factor on efficient mineralization, and then tackle how fluid evolution regulates molybdenum isotope fractionation. Molybdenites, which preferentially partition isotopically light Mo (Rayleigh fractionation), precipitated from a single fluid will develop a heavier  $\delta^{98/95}\text{Mo}$  composition over time, and this also creates heterogeneous  $\delta^{98/95}\text{Mo}$  between molybdenite grains. Whereas a fluid undergoing multiple episodes of intensive boiling will gradually lose its isotopically heavy Mo to the vapor phase, molybdenites crystallizing successively from the residual liquid will then have lighter  $\delta^{98/95}\text{Mo}$  over time. However, when mineralization efficiency becomes too low, a negligible variation in  $\delta^{98/95}\text{Mo}$  of molybdenite is observed. Given that the mineralization efficiency (i.e., the amount of Mo crystallized as molybdenite from the fluid) rarely reaches 100% and molybdenite favors isotopically light Mo, the presence of a residual fluid with isotopically heavy Mo is inevitable. This residual fluid may then become trapped in alteration halos; hence,  $\delta^{98/95}\text{Mo}$  has the potential to aid in locating the mineralization center (e.g., lighter  $\delta^{98/95}\text{Mo}$  toward the orebody). The residual fluid may also feed surface hydrological systems and eventually impact Mo cycling. Our study highlights that understanding the controls of isotope fractionation is critical to bridge the gap between ore formation and elemental cycling, and that other transition metals (e.g., Cu, Fe, and Zn) may follow similar trajectories.

### Introduction

Molybdenum is important to an industrialized society because of its critical role in the steel industry. One of the predominant sources of Mo is molybdenite-bearing porphyry deposits within the upper continental crust (Sillitoe, 2010). Owing to the redox sensitivity of Mo, its isotopic composition in marine sediments is also a powerful proxy for quantitatively reconstructing the distribution of oxic and anoxic conditions in past oceans (Dickson, 2017; Kendall et al., 2017). Therefore, understanding the mechanisms controlling Mo enrichment and the associated isotope fractionation in porphyry deposits (Fig. 1) is vital because they (1) underpin genetic models of porphyry deposit formation (Sillitoe, 2010; Richards, 2011; Kouzmanov and Pokrovski, 2012), (2) provide important boundary conditions for estimating  $\delta^{98/95}\text{Mo}$  of the upper continental crust (Hannah et al., 2007; Greber et al., 2014; Breillat et al., 2016), and (3) constrain Mo cycling in surface environments, which is essential when utilizing  $\delta^{98/95}\text{Mo}$  of marine sediments as a paleoredox proxy (Dickson, 2017; Kendall et al., 2017).

Metalliferous aqueous fluids that form porphyry deposits are exsolved from magmatic reservoirs at the base of the

upper crust (Kouzmanov and Pokrovski, 2012; Wilkinson, 2013; Chelle-Michou et al., 2017; Chiaradia and Caricchi, 2017). After exsolution, these magmatic aqueous fluids migrate upward and may undergo decompression, boiling, cooling, and fluid mixing (Driesner and Heinrich, 2007; Richards, 2011; Kouzmanov and Pokrovski, 2012; Cooke et al., 2014). Among these processes, decompression-induced phase separation is a key factor controlling the formation of porphyry deposits (Richards, 2011; Cooke et al., 2014). During pressure release-induced boiling, a single-phase magmatic aqueous fluid separates into liquid and vapor phases with contrasting physicochemical properties (e.g., density and composition). The vapor phase tends to migrate to shallow depths due to its low density, while the liquid phase preferentially accumulates in deeper parts of the hydrothermal system, giving rise to different mineralization styles (Zajacz et al., 2017). Despite being extensively studied, the transportation, precipitation, and accompanying isotope fractionation mechanisms of Mo during this process are poorly established. Based on experimental studies (Rempel et al., 2006) and variations in Mo isotopes (>0.63‰ per atomic mass unit) documented in Mo-bearing porphyry deposits (Hannah et al., 2007), Mo has been assumed to be transported in the vapor phase, with

<sup>†</sup>Corresponding author: e-mail, geoliy@outlook.com; geoliy@mail.iggcas.ac.cn

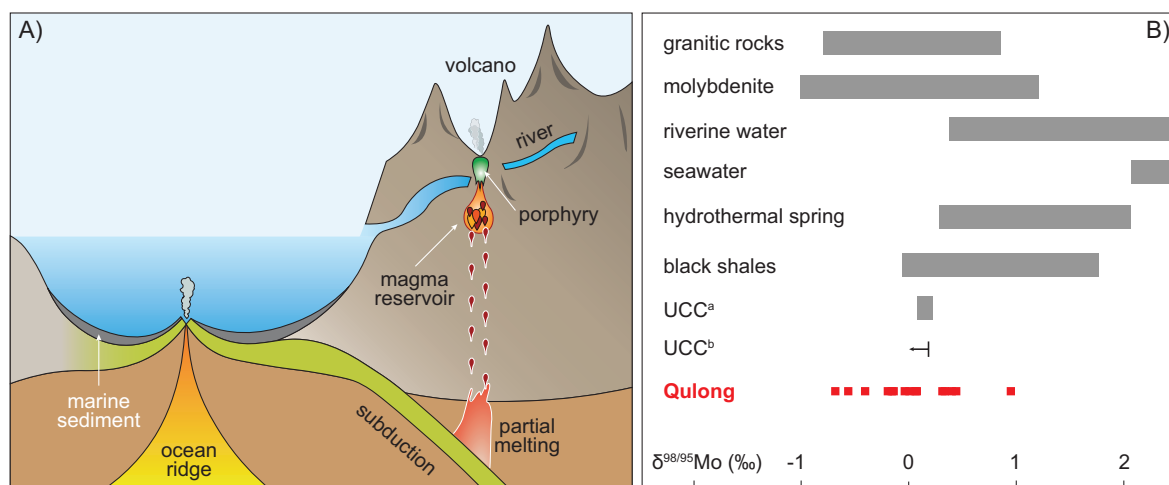


Fig. 1. A) Schematic model describing Mo cycling in the upper continental crust. The most significant redistribution of Mo in the upper continental crust is represented by the circulation of aqueous fluid at convergent margins. This Mo is mainly hosted by molybdenite-bearing porphyry deposits. During weathering and erosion, Mo will enter the oceans through river transfer and eventually get locked in marine organic-rich sediments. B) The  $\delta^{98/95}\text{Mo}$  of relevant geologic reservoirs in the surface environment, modified after Willbold and Elliott (2017). Data for hydrothermal springs are from Neely et al. (2018). Two estimates of the upper continental crust (UCC<sup>a</sup> and UCC<sup>b</sup>) are identical within individual uncertainties (Greber et al., 2014; Willbold and Elliott, 2017).

molybdenite being precipitated when there is a reduction in oxygen fugacity and temperature. However, a recent experimental study suggests that Mo can be efficiently withheld in the liquid phase during phase separation and favors a scenario of liquid transportation (Zajacz et al., 2017), which is in line with the enrichment of Mo in brine-rich fluid inclusions at the Questa porphyry Mo deposit (Klemm et al., 2008). With a robust understanding of Mo isotope fractionation in porphyry deposits, it is also possible to utilize Mo isotopes as a proxy to locate the mineralization center.

Here, we explore the factors controlling  $\delta^{98/95}\text{Mo}$  in molybdenite in porphyry deposits and discuss the implications for Mo cycling in the surface environment through the study of the Tibetan Qulong porphyry Cu-Mo deposit. The Qulong deposit is a very good candidate for this purpose given that it has been exceptionally well characterized in previous studies (Yang et al., 2009; Hu et al., 2015; Zhao et al., 2016a; Li et al., 2017a, b, 2018) and therefore allows for an evaluation of the factors controlling  $\delta^{98/95}\text{Mo}$  evolution during the ore-forming process and yields implications for our understanding of ore formation and elemental cycling.

### Deposit Geology and Samples

The Qulong porphyry Cu-Mo deposit, situated at the southwest margin of the Lhasa terrane, southern Tibet (Fig. 2A), is a representative porphyry deposit from the Gangdese porphyry copper belt formed in a postcollisional setting (Hou et al., 2009; Wang et al., 2018). This giant deposit contains >2,200 million tonnes of ore with an average grade of 0.5% and 0.03% for Cu and Mo, respectively (Li et al., 2017b). Most of the mineralization assemblages at Qulong are hosted by the  $17.142 \pm 0.023$  Ma ( $2\sigma$ , with analytical and decay constant uncertainties) Rongmucuola pluton, which has a granodioritic-monzogranitic composition (Fig. 2B; Li et al., 2017a). Additional mineralization is associated with the Jurassic Yeba Formation volcanic rocks (Yang et al., 2009; Li et al., 2017b). Field observations

and chronological studies suggest that mineralization at Qulong was broadly coeval with the emplacement of the  $16.009 \pm 0.024$  Ma intermineral P porphyry and, to a lesser extent, with

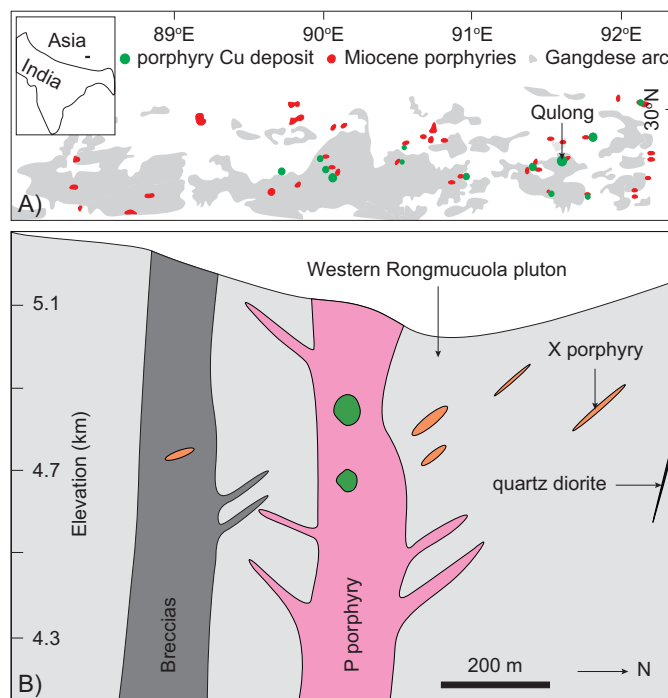


Fig. 2. A) Distribution of Miocene porphyries and porphyry Cu deposits in the Gangdese magmatic arc. Inset shows the position of the Gangdese magmatic arc relative to the plate boundary between India and Asia. B) Cross section illustrating the deposit geology of the Qulong porphyry Cu-Mo deposit. The mineralization at Qulong is primarily hosted by the pre-ore Rongmucuola pluton, with mineralization being directly linked to the intermineral P porphyry and, to a lesser extent, the X porphyry. A syn-ore hydrothermal breccia is also developed, and the cessation of magmatism is marked by the post-ore quartz diorite.

the syn-ore X porphyry, which is slightly younger than the P porphyry (Yang et al., 2009; Hu et al., 2015; Zhao et al., 2016a; Li et al., 2017a). A syn-ore hydrothermal breccia pipe comprising two stages of breccia is documented. The breccia pipe is inferred to be slightly younger than the X porphyry (Yang et al., 2009; Li et al., 2017a). The Rongmucuola pluton was intruded by a post-ore diorite, which has a crystallization age of  $15.166 \pm 0.020$  Ma (Li et al., 2017a).

High-precision Re-Os molybdenite geochronology suggests that the bulk of mineralization at Qulong was formed in three intermittent mineralization pulses at 16.126 to 16.050, 16.040 to 15.981, and 15.981 to 15.860 Ma, respectively (Li et al., 2017a). In agreement with field geology, fluid inclusion, and oxygen isotope studies (Yang et al., 2009; Li et al., 2017b, 2018), the three mineralization pulses are characterized by rapid cyclic cooling ( $>0.55^\circ\text{C}/1,000$  yr), with temperatures fluctuating at  $425^\circ$  to  $360^\circ$ ,  $365^\circ$  to  $290^\circ$ , and  $345^\circ$  to  $285^\circ\text{C}$ , respectively. Fluid evolution is constrained over an absolute time frame and is interpreted to illustrate that the amount of metals being deposited in the three mineralization pulses progressively decreases, with the majority of the mineralization (i.e.,  $>60\%$ ) occurring in the first mineralization pulse (Li et al., 2018). Evidence of fluid boiling is observed in the premineralization-stage barren quartz veins and a two-stage metalliferous syn-ore breccia pipe (Yang et al., 2009; Li et al., 2017b). Rapid cooling initiated by mixing hot magmatic fluid with cold meteoric water has been proposed to be the main trigger of metal deposition (Li et al., 2018).

To characterize the controls on Mo isotope composition during the ore-forming process in magmatic-hydrothermal systems and to use this to yield implications in elemental cycling, 12 quartz-molybdenite veins (20 samples) previously studied by Li et al. (2017a) were investigated for  $\delta^{98/95}\text{Mo}$ . These samples are ideal for the aims of this research because their mineralization stage, alteration assemblages, formation age, temperature, and associated fluid source have been well characterized through core logging, high-precision (1,000-yr resolution) Re-Os molybdenite chronology, fluid inclusion, and ion probe quartz oxygen isotope studies (Li et al., 2017a, b, 2018).

Previous studies have documented variation in  $\delta^{98/95}\text{Mo}$  at the hand-specimen scale (Greber et al., 2014). To advance our understanding of the controls on  $\delta^{98/95}\text{Mo}$  at the centimeter scale, we have investigated how sample size affects  $\delta^{98/95}\text{Mo}$ . To do so, we analyzed samples of variable digestion masses and tracked  $\delta^{98/95}\text{Mo}$  variations along single molybdenite veins. In the former technique, a coarse-grained molybdenite sample (2 mm, sample 1605-80/6-7) and a fine-grained molybdenite sample (0.2 mm, sample 1605-80/2-7) were obtained as independent aliquots from the same vein. For the latter technique, multiple independent molybdenite separates were obtained from a single molybdenite vein; these were assumed to form rapidly at a timescale that is unresolvable by current high-precision dating ( $<0.008$  m.y.; Li et al., 2017a). Three veins from different mineralization stages were investigated here for such a purpose (1605-80, 1605-268, and 1605-155).

Two whole-rock samples (1605-80 and QL03) that show least evidence of mineralization were analyzed to constrain the  $\delta^{98/95}\text{Mo}$  composition of ore-related magma at Qulong. Sample 1605-80 belongs to the Rongmucuola pluton, which

has a granodioritic composition, and sample QL03 belongs to the P porphyry, which is a monzogranite.

### Analytical Methods

Molybdenite samples utilized here were studied previously by Li et al. (2017a) and were recovered as whole grains by an HF leaching method (Lawley and Selby, 2012). We suggest that the HF method has no impact on the  $\delta^{98/95}\text{Mo}$  of molybdenite for two reasons. First, no molybdenite dissolution was observed; second, the Re-Os molybdenite system displays a closed-system behavior during the leaching process (Lawley and Selby, 2012; Li et al., 2017a). This argument is also consistent with the homogeneous  $\delta^{98/95}\text{Mo}$  composition along single molybdenite-bearing veins (see below for detailed discussion).

Aliquots of purified molybdenite were weighed and sample digestion was achieved in 2 ml of 16-M  $\text{HNO}_3$  and 1 ml of 12-M  $\text{HCl}$  at  $150^\circ\text{C}$  for 48 h. Once completely digested, the solution was dried at  $60^\circ\text{C}$  and then completely redissolved in 1 ml of 1-M  $\text{HNO}_3$ . A portion of the redissolved sample, equivalent to 300 ng of natural Mo, was aliquoted and spiked with a  $^{97}\text{Mo}$ - $^{100}\text{Mo}$  double spike. The spiked sample solution was brought up to 1 ml by adding 16-M  $\text{HNO}_3$ . Molybdenum isotope equilibrium between sample and spike was achieved at  $150^\circ\text{C}$  for at least 24 h. The sample was then dried and converted to chloride form for anion-exchange chromatography. Chemical separation of Mo from the matrix was carried out using a single-pass anion exchange procedure (Pearce et al., 2009; Neely et al., 2018). The columns containing 2 ml of Bio-Rad AG1-X8 resin were precleaned successively with 8-M  $\text{HNO}_3$ , 6-M  $\text{HCl}$ , 1-M  $\text{HCl}$ , 1-M  $\text{HF}$ , and 3-M  $\text{HNO}_3$  and then conditioned in 0.5-M  $\text{HCl}$ . The samples were loaded to the columns in 5 ml of 0.5-M  $\text{HCl}$ , and a bulk wash was undertaken with 10 ml of 0.5-M  $\text{HCl}$  + 1-M  $\text{HF}$  and 8 ml of 4-M  $\text{HCl}$ . Then, an additional matrix elution step of 10 ml of 1-M  $\text{HF}$  was added to ensure complete Zn removal prior to the collection of Mo in 12 ml of 3-M  $\text{HNO}_3$ . Total procedural blanks for processing Mo in this study were 0.2 to 1.5 ng ( $n = 2$ ), which are comparable to the long-term blanks at Durham University ( $\sim 1$  ng) and negligible in comparison to the total amount of sample processed (i.e., 300 ng natural Mo).

Molybdenum isotope analyses were conducted using a Thermo Scientific Neptune multicollector-inductively coupled plasma-mass spectrometer in the Arthur Holmes Laboratories at Durham University. Samples were introduced to the instrument using an Aridus II desolvator and a Savillex PFA20 nebulizer in 0.5-M  $\text{HNO}_3$  at 150- to 200-ppb concentrations. The data were processed using IsoSpike (Creech and Paul, 2015), which is an add-in to the Iolite data processing package (Paton et al., 2011). All analyses herein were measured relative to the international reference solution SRM NIST3134 (Greber et al., 2012; Goldberg et al., 2013) and have been normalized so that  $\delta^{98/95}\text{Mo}_{\text{NIST}}$  equals 0‰. Molybdenum isotope composition data are expressed using conventional  $\delta$  notation in parts per thousand relative to the reference standard, whereby

$$\delta^{98/95}\text{Mo} = \left( \frac{{}^{98}\text{Mo}/{}^{95}\text{Mo}_{\text{sample}} - {}^{98}\text{Mo}/{}^{95}\text{Mo}_{\text{NIST3134}}}{{}^{98}\text{Mo}/{}^{95}\text{Mo}_{\text{NIST3134}}} \right) \cdot 1,000. \quad (1)$$

Analytical and instrumental mass fractionations were corrected using the  $^{97}\text{Mo}$ - $^{100}\text{Mo}$  double spike. Mass spectrometer

drift and long-term reproducibility of the data were monitored by measuring Mo isotope standards, including Romil and OU (Open University). The obtained  $\delta^{98/95}\text{Mo}$  values of Romil ( $0.04 \pm 0.03\%$ ,  $n = 41$ , 2 standard deviations [SD]) and OU ( $-0.34 \pm 0.04\%$ ,  $n = 9$ , 2 SD) were indistinguishable from previously published values, within analytical uncertainties (Goldberg et al., 2013; Neely et al., 2018).

The reproducibility of  $\delta^{98/95}\text{Mo}$  values in the molybdenite samples was further evaluated using three international Re-Os molybdenite age reference materials: JDC, HLP-5, and NIST RM8599 (Table 1; Du et al., 2004; Markey et al., 2007). The obtained  $\delta^{98/95}\text{Mo}$  values of the NIST RM8599 (Henderson), JDC, and HLP-5 were  $-0.11 \pm 0.01\%$  ( $n = 9$ , 2 SD),  $-0.02 \pm 0.04\%$  ( $n = 9$ , 2 SD), and  $-0.61 \pm 0.02\%$  ( $n =$

9, 2 SD), respectively, which are the same within uncertainties as previous studies (Siebert et al., 2001; Malinovsky et al., 2005; Breillat et al., 2016; Zhao et al., 2016b). An additional in-house molybdenite Re-Os age control sample, 2706.SWB, from Endako porphyry Mo deposit, British Columbia, Canada (Selby and Creaser, 2001), yielded a value of  $-0.55 \pm 0.04\%$  (Table 1;  $n = 10$ , 2 SD). Conservatively, the long-term reproducibility of  $\delta^{98/95}\text{Mo}$  analyses herein is considered to be  $\leq 0.05\%$  (2 SD).

## Results

### Mo isotope heterogeneity at centimeter scale

We first evaluated the effects of digestion mass on the reproducibility of  $\delta^{98/95}\text{Mo}$  (Table 2). For fine-grained molybdenite (0.2 mm, sample 1605-80/2-7), reproducible  $\delta^{98/95}\text{Mo}$  data (Fig. 3A) were not obtained until the digestion mass was  $>5$  mg (i.e.,  $\geq 20$  grains). For coarse-grained molybdenite (2 mm, sample 1605-80/6-7), homogeneous  $\delta^{98/95}\text{Mo}$  values were obtained regardless of digestion mass (1, 5, and  $>80$  grains, equivalent to 0.8, 4.1, and 70 mg, respectively; Fig. 3B). Therefore, for the remaining analyses, sufficient molybdenite (i.e., 10–70 mg) was dissolved to yield representative  $\delta^{98/95}\text{Mo}$ . We also investigated the variation in  $\delta^{98/95}\text{Mo}$  along individual quartz-molybdenite veins (Table 3). Multiple independent molybdenite aliquots from three different veins representing temporally distinct mineralization stages (sample 1605-80, 1605-268, 1605-155) were analyzed. All of them yielded homogeneous  $\delta^{98/95}\text{Mo}$  values within the vein (Fig. 3C-E).

### Time-resolved Mo isotope evolution at Qulong

Twenty samples covering the entire mineralization sequence at Qulong show pronounced variations in  $\delta^{98/95}\text{Mo}$ : values range between  $-0.68$  and  $+0.95\%$  (Table 4). However,  $\delta^{98/95}\text{Mo}$  shows no clear dependence on either temperature or meteoric water contribution inferred from  $\delta^{18}\text{O}$  data (Fig. 4A, B; Li et al., 2018). The first mineralization pulse (16.126–16.050 Ma) shows decreasing  $\delta^{98/95}\text{Mo}$ , from  $+0.95$  to  $-0.68\%$ , through time ( $n = 4$ , Fig. 5). The second mineralization pulse (16.040–15.981 Ma), with exception of two veins that have higher  $\delta^{98/95}\text{Mo}$  ( $-0.16$  and  $+0.44\%$ ), yields gradually increasing  $\delta^{98/95}\text{Mo}$ , from  $-0.56$  to  $+0.32\%$  ( $n = 5$ ). The third mineralization pulse (15.981–15.860 Ma) has relatively invariant  $\delta^{98/95}\text{Mo}$  of  $-0.02$  to  $+0.08\%$  ( $n = 6$ ).

### Magmatic rocks at Qulong

The Mo isotope composition of two apparently poorly mineralized igneous rocks was also investigated. Sample QL03 from the P porphyry has a  $\delta^{98/95}\text{Mo}$  of  $-0.21 \pm 0.02\%$  ( $n = 5$ ). However, given it has an Mo concentration of 425 ppm and contains disseminated molybdenite as confirmed petrographically, it should reflect the  $\delta^{98/95}\text{Mo}$  of mineralization instead of representing the primary  $\delta^{98/95}\text{Mo}$  of igneous rocks at Qulong. Sample 1605-80 from the Rongmucuola pluton contains only 2.45 ppm Mo (at upper end of global granites; Yang et al., 2017) and possesses a  $\delta^{98/95}\text{Mo}$  of  $0.34 \pm 0.04\%$  ( $n = 5$ ), which provides our best estimate of the  $\delta^{98/95}\text{Mo}$  of the original igneous rocks at Qulong. Due to the potential impact on the  $\delta^{98/95}\text{Mo}$  of igneous rocks by hydrothermal alteration and mineralization, these data are not discussed further.

Table 1. Molybdenum Isotope Composition of Commonly Used Molybdenite Re-Os Age Standards

Standard	Run no.	$\delta^{98/95}\text{Mo}$ (‰)	$2\sigma^1$	Average	2 SD <sup>1</sup>
<b>Molybdenite standards</b>					
HLP	HLP_1	-0.62	0.01	-0.61	0.02
	HLP_2	-0.62	0.02		
	HLP_3	-0.60	0.02		
	HLP_4	-0.61	0.02		
	HLP_5	-0.60	0.01		
	HLP(2)_6	-0.61	0.02		
	HLP(2)_7	-0.61	0.02		
	HLP(2)_8	-0.62	0.02		
	HLP(2)_9	-0.60	0.02		
JDC	JDC_1	-0.01	0.02	-0.02	0.04
	JDC_2	-0.04	0.02		
	JDC_3	0.01	0.02		
	JDC_4	0.00	0.02		
	JDC_5	0.00	0.02		
	JDC(2)_6	-0.04	0.02		
	JDC(2)_7	-0.03	0.02		
	JDC(2)_8	-0.02	0.02		
	JDC(2)_9	-0.01	0.02		
Henderson_NIST	NIST_1	-0.12	0.02	-0.11	0.01
	NIST_2	-0.11	0.02		
	NIST_3	-0.11	0.02		
	NIST_4	-0.12	0.02		
	NIST_5	-0.10	0.01		
	NIST(2)_6	-0.12	0.02		
	NIST(2)_7	-0.11	0.02		
	NIST(2)_8	-0.11	0.02		
	NIST(2)_9	-0.12	0.02		
2706.SWB	SWB_1	-0.56	0.02	-0.55	0.04
	SWB_2	-0.57	0.02		
	SWB_3	-0.54	0.01		
	SWB_4	-0.56	0.02		
	SWB_5	-0.53	0.01		
	SWB(2)_6	-0.52	0.01		
	SWB(2)_7	-0.58	0.02		
	SWB(2)_8	-0.55	0.02		
	SWB(2)_9	-0.53	0.02		
	SWB(2)_10	-0.55	0.02		

Notes: For each digested sample, two separate aliquots were spiked and processed through chemistry; multiple analyses were conducted by multi-collector-inductively coupled plasma-mass spectrometry, and the standard deviation on the average was calculated from all individual analyses

<sup>1</sup> $2\sigma$  refers to the two standard deviations of multiple instrumental analyses of the same standard solution (i.e., measuring the same solution several times), while 2 SD is the two standard deviations of multiple independent analyses of the same standard (e.g., multiple solutions from digesting the same standard)

Table 2. Testing Digestion Masses as a Controlling Factor on  $\delta^{98/95}\text{Mo}$ 

Sample no.	Aliquot	No. of grains	Weight (mg)	$\delta^{98/95}\text{Mo}$ (‰)	$2\sigma^1$	No. of analyses
1605-80/2-7	A	>80 grains	18.0	-0.15	0.02	2
	B	20 grains	4.6	-0.12	0.03	3
	C	8 grains	1.3	0.01	0.03	3
	D	4 grains (0.2 mm)	0.4	-0.08	0.03	3
1605-80/6-7	A	>80 grains (1–2 mm)	70.0	-0.14	0.02	2
	B	5 grains (2 mm)	4.1	-0.13	0.01	2
	C	1 grain (2 mm)	0.8	-0.12	0.04	2

<sup>1</sup>For each digested sample, multiple analyses were conducted by multicollector-inductively coupled plasma-mass spectrometry for the same solution, and the  $2\sigma$  were two standard deviations of these analyses

Table 3. Homogeneous  $\delta^{98/95}\text{Mo}$  Along Single Quartz-Molybdenite Veins

Vein	Vein fraction	Weight (mg)	$\delta^{98/95}\text{Mo}$ (‰)	$2\sigma^1$	No. of analyses	Average	2 SD <sup>1</sup>
1605-80	1605-80/2-7	18.0	-0.15	0.02	2	-0.15	0.02
	1605-80/4-7	48.1	-0.17	0.04	2		
	1605-80/6-7	70.0	-0.14	0.02	2		
	1605-80/7-7	26.1	-0.16	0.01	2		
1605-268	1605-268/1-3	22.9	0.31	0.05	2	0.32	0.02
	1605-268/2-3	18.8	0.32	0.01	2		
	1605-268/3-3	23.6	0.34	0.00	2		
1605-155	1605-155/1-4	25.7	-0.04	0.02	2	-0.02	0.04
	1605-155/2-4	37.2	-0.02	0.01	2		
	1605-155/3-4	32.4	-0.03	0.02	2		
	1605-155/4-4	28.9	0.01	0.01	2		

<sup>1</sup> $2\sigma$  refers to the two standard deviations of multiple instrumental analyses of a single sample (i.e., measuring the same solution several times), while 2 SD is the two standard deviations of multiple samples (e.g., several samples along a single vein)

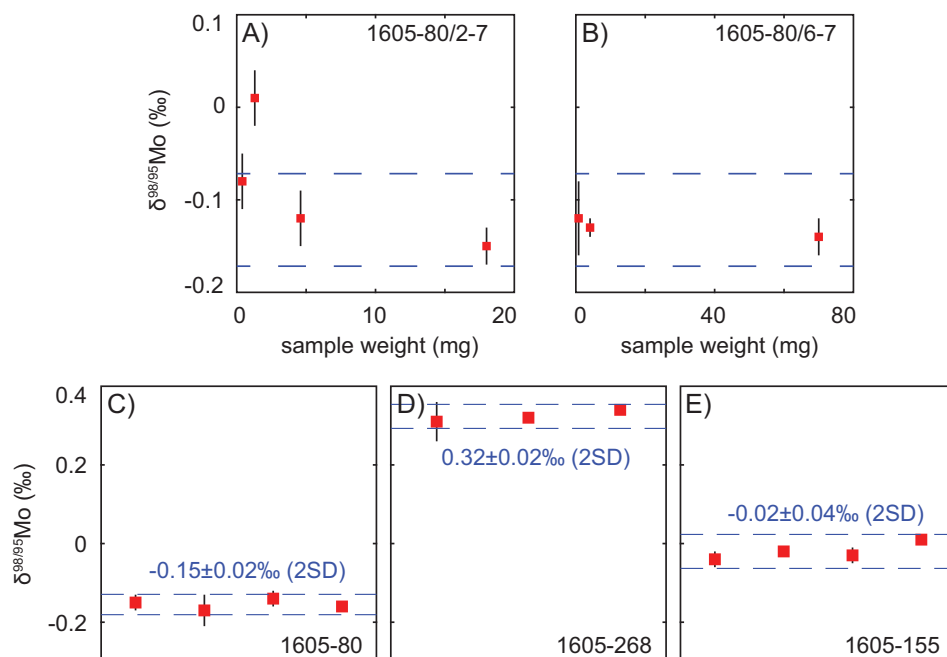


Fig. 3. A, B) The effects of variable digestion masses on Mo isotope composition. The two samples (1605-80/2-7 and 1605-80/6-7) were aliquots separated independently from the same molybdenite vein (1605-80). For sample 1605-80/2-7, which comprises fine-grained (0.2 mm) molybdenite grains, reproducible  $\delta^{98/95}\text{Mo}$  values were not obtained until the digestion masses were >5 mg (i.e., >20 grains). In contrast, the  $\delta^{98/95}\text{Mo}$  values of the coarse-grained (2 mm) sample 1605-80/6-7 were reproducible regardless of digestion mass. The dashed blue lines represent the recommended  $\delta^{98/95}\text{Mo}$  of sample 1605-80 at  $2\sigma$  level. C-E) Multiple aliquots independently separated from single molybdenite veins were studied to test the homogeneity of  $\delta^{98/95}\text{Mo}$  along single molybdenite veins. The three molybdenite veins (1605-80, 1605-268, and 1605-155) investigated here all yield homogeneous  $\delta^{98/95}\text{Mo}$ . Abbreviation: SD = standard deviation.

Table 4.  $\delta^{9895}\text{Mo}$  of 12 Quartz-Molybdenite Veins<sup>1</sup> and Two Igneous Rocks at Qulong

Sample no.	Sample weight (mg)	$\delta^{9895}\text{Mo}$		No. of analyses	Mineralization pulses	Formation age <sup>2</sup>		Formation temperature <sup>3</sup> °C	Quartz $\delta^{18}\text{O}_{\text{quartz}}^4$		Ore-forming fluid $\delta^{18}\text{O}_{\text{fluid}}$ and magmatic water % <sup>4</sup>				
		‰	$2\sigma^5$			Ma	$2\sigma$		‰	$2\sigma$	‰	$2\sigma$	Value	$2\sigma$	
Molybdenites															
313-145 <sup>6</sup>	0.54	0.95	0.05	4	1st pulse	16.126	0.008	425	20	8.27	0.45	4.7	0.6	87.6	5.0
313-460	10.7	0.40	0.05	4		16.107	0.015	398	20	9.20	0.47	5.1	0.6	89.2	5.1
001-640	16.5	-0.40	0.01	4		16.098	0.013	390	20	11.90	0.51	7.6	0.7	100.0	5.3
1402-209 <sup>6</sup>	8.9	-0.68	0.02	3		16.088	0.007	380	20	9.95	0.42	5.4	0.6	90.7	5.1
1605-80/2-7	18.0	-0.15	0.02	2	2nd pulse	16.050	0.005	360	20	8.12	0.47	3.1	0.7	80.5	5.6
1605-80/4-7	48.1	-0.17	0.04	2		16.050	0.005	360	20	8.12	0.47	3.1	0.7	80.5	5.6
1605-80/6-7	70.0	-0.14	0.02	2		16.050	0.005	360	20	8.12	0.47	3.1	0.7	80.5	5.6
1605-80/7-7	26.1	-0.16	0.01	2		16.050	0.005	360	20	8.12	0.47	3.1	0.7	80.5	5.6
1405-120	14.1	-0.56	0.02	2		16.040	0.007	365	20	8.81	0.42	3.9	0.7	84.1	5.3
1605-70	17.4	0.44	0.01	2		16.036	0.012	365	20	9.12	0.39	4.2	0.6	85.4	5.2
1605-334	37.1	-0.19	0.02	2		16.011	0.015	340	20	8.83	0.36	3.2	0.7	81.2	5.5
1605-268/1-3	22.9	0.31	0.05	2		15.981	0.007	290	20	9.24	0.28	2.0	0.8	75.8	6.2
1605-268/2-3	18.8	0.32	0.01	2		15.981	0.007	290	20	9.24	0.28	2.0	0.8	75.8	6.2
1605-268/3-3	23.6	0.34	0.00	2		15.981	0.007	290	20	9.24	0.28	2.0	0.8	75.8	6.2
1605-155/1-4	25.7	-0.04	0.02	2	3rd pulse	15.943	0.007	345	20	9.03	0.39	3.6	0.7	82.7	5.5
1605-155/2-4	37.2	-0.02	0.01	2		15.943	0.007	345	20	9.03	0.39	3.6	0.7	82.7	5.5
1605-155/3-4	32.4	-0.03	0.02	2		15.943	0.007	345	20	9.03	0.39	3.6	0.7	82.7	5.5
1605-155/4-4	28.9	0.01	0.01	2		15.943	0.007	345	20	9.03	0.39	3.6	0.7	82.7	5.5
1605-53	22.3	0.08	0.04	2		15.939	0.006	310	20	8.92	0.40	2.4	0.8	77.5	6.0
1605-33	10.5	0.07	0.01	2		15.860	0.010	285	20	9.46	0.44	1.8	0.9	75.1	6.5
Whole rocks															
QL03	500.0	-0.21	0.02	5	Rongmucuoia pluton	17.142	0.014	-	-	-	-	-	-	-	-
QL1605-80	500.0	0.34	0.04	5	P porphyry	16.009	0.017	-	-	-	-	-	-	-	-

<sup>1</sup>Formation ages, temperatures, and estimations of fluid  $\delta^{18}\text{O}$  and magmatic water contributions for these veins are also presented

<sup>2</sup>Formation ages are constrained by isotope dilution-thermal ionization mass spectrometry molybdenite Re-Os and zircon U-Pb geochronology; see Li et al. (2017a) for further details

<sup>3</sup>Formation temperatures are constrained by trapping temperatures of fluid inclusion assemblages; see Li et al. (2017b) for further details

<sup>4</sup>Oxygen isotopes of quartz and ore-forming fluids, with inferred contributions of magmatic water; see Li et al. (2018) for further details

<sup>5</sup>For each digested sample, multiple analyses were conducted by multicollector-inductively coupled plasma-mass spectrometry, and  $2\sigma$  is two standard deviations of these analyses

<sup>6</sup>For samples 313-145 and 1402-209, only 0.5 and 8.9 mg of molybdenite were available

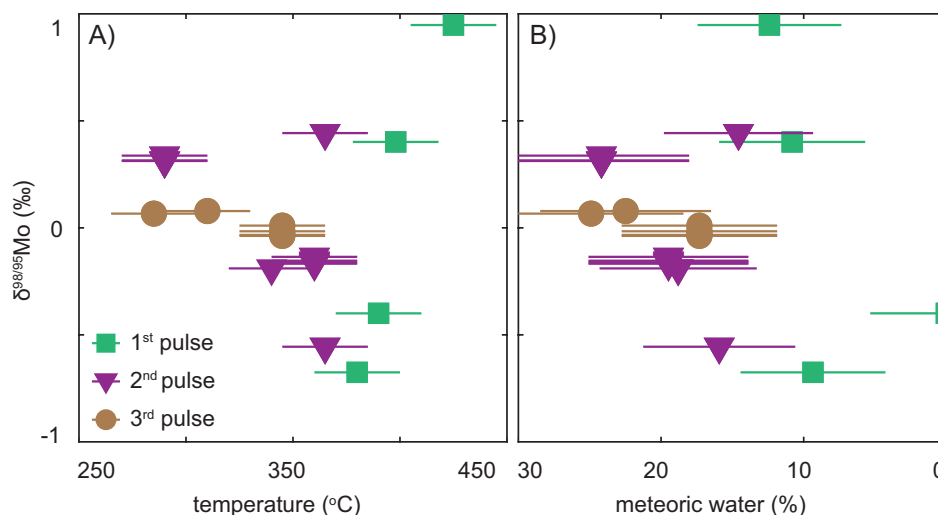


Fig. 4. A, B) The Mo isotope composition at Qulong shows no correlation with temperature or the proportion of meteoric water. The corresponding temperatures and contributions of meteoric water of the molybdenite veins were constrained through fluid inclusion and secondary ion mass spectrometry oxygen isotope studies of hydrothermal quartz grains coprecipitated with this molybdenite (Li et al., 2017b, 2018). Samples are divided based on mineralization pulse with the different pulses from first to third comprising 4, 10, and 6 samples, respectively.

## Discussion

### *Fluid mixing facilitated rapid cooling as an efficient driver of mineralization*

The formation of porphyry deposits requires efficient transportation of metals in their oxidized states by hydrothermal fluids, before being rapidly reduced to sulfides (Richards, 2011; Kouzmanov and Pokrovski, 2012; Sun et al., 2013; Cooke et al., 2014). The molybdenite-bearing veins studied here were formed at ~25 MPa (~2.5 km at hydrostatic pressure) and 280° to 425°C (Li et al., 2017b). These conditions are similar to those commonly reported for porphyry deposit formation worldwide (Richards, 2011; Kouzmanov

and Pokrovski, 2012; Cooke et al., 2014). Critically, these temperature-pressure conditions mark the region where a metaliferous aqueous fluid changes its chemical-physical state between the supercritical state and liquid and vapor phases (Driesner and Heinrich, 2007). Aqueous fluid in its supercritical state is characterized by high metal solubility (Kessel et al., 2005); therefore, these conditions are favorable for the efficient transportation of metals. For example, it has been reported that up to 500 ppm Mo is soluble at 420°C (Klemm et al., 2008). During the formation of porphyry deposits, hydrothermal fluids need to be cooled from >600° to <450°C (Richards, 2011; Kouzmanov and Pokrovski, 2012; Cooke et al., 2014). Recent advances in constraining the timescale of

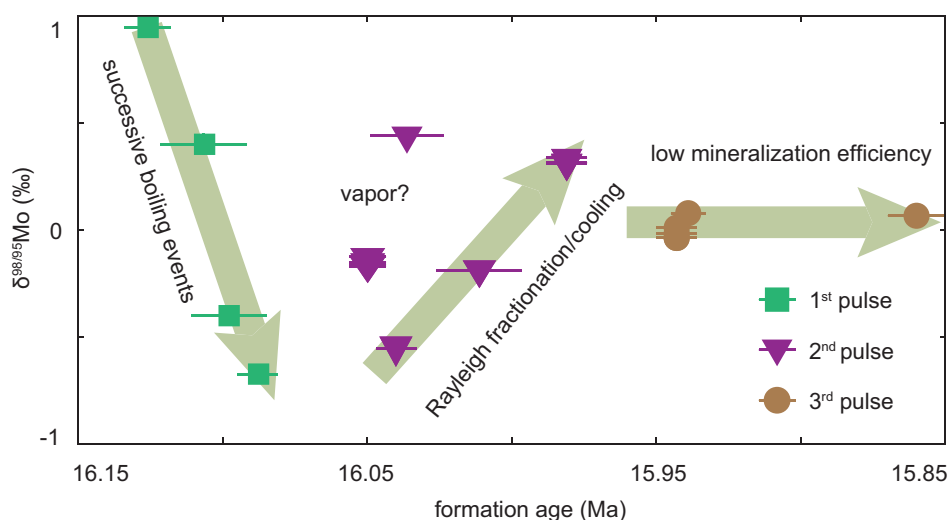


Fig. 5. Time-resolved Mo isotope composition evolution of the three mineralization pulses at Qulong. The time frame and three inferred mineralization pulses were derived from high-precision molybdenite Re-Os geochronology (Li et al., 2017a). Molybdenite veins from the first mineralization pulse display decreasing  $\delta^{98/95}\text{Mo}$  through time, while the second mineralization pulse is characterized by an increasing  $\delta^{98/95}\text{Mo}$  trend, except for two veins that fall off this trend with higher values. The third mineralization pulse has relatively invariant  $\delta^{98/95}\text{Mo}$ .

magmatic-hydrothermal system development indicate that porphyry systems are formed through multiple short-lived pulses over a few to tens of thousands of years (Mercer et al., 2015; Spencer et al., 2015; Buret et al., 2016; Li et al., 2017a). Rapid cooling is a necessity for ore formation. Upon cooling, the aqueous fluid enters the liquid state. This is accompanied by a significant drop in metal solubility; hence, efficient sulfide precipitation is expected (Kouzmanov and Pokrovski, 2012). This scenario is in line with the observation at Qulong that >60% metals were deposited within ~38 k.y.—an interval when temperatures dropped from >425° to <360°C (Li et al., 2018). Similarly, a significant decrease in the metal content of ore-forming fluids upon cooling occurred at Bingham, Morococha, and the Questa porphyry deposits, when the temperature of the fluids decreased from ~450° to ~300°C (Landtwing et al., 2005; Klemm et al., 2008; Kouzmanov and Pokrovski, 2012). Collectively, this suggests that cooling is an important mechanism for metal deposition in porphyry deposits.

The short timescales required for ore formation and the rapid cooling needed for metal deposition require a mechanism that can generate a large temperature gradient. Significant thermal contributions come from magma and fluid fluxes in cyclic systems (Mercer et al., 2015; Li et al., 2017a); thus, it is critical to have an efficient cooling mechanism. Given its low efficiency, thermal conduction cannot be the primary driver for cooling (Weis et al., 2012). Here, we explore the possibility of mixing hot magmatic fluid and cold meteoric water to facilitate efficient mineralization in porphyry systems. At Qulong, time-resolved fluid evolution provides quantitative constraints on the amount of meteoric water involved in the ore-forming process (Li et al., 2018). Assuming magmatic fluid and meteoric water have temperatures of ~600° and 20°C, respectively, mixing magmatic fluid with 10% meteoric water will yield a hydrothermal fluid with a temperature of ~488°C, with the temperature falling to ~376°C for a hydrothermal fluid bearing 20% meteoric water. These temperatures and meteoric water contributions are in excellent agreement with observations at Qulong (Li et al., 2017b, 2018). More importantly, the temperature drop associated with fluid mixing happens almost instantly. In tandem with the ubiquitous involvement of meteoric water in porphyry deposits (Fekete et al., 2016; Li et al., 2018), we argue that rapid cooling facilitated by mixing of hot magmatic and cold meteoric water is a primary driver for metal deposition.

#### *Grain-scale Mo isotope heterogeneity governed by Rayleigh fractionation*

Previous studies have shown that significant Mo isotope fractionation occurs during both fluid evolution and molybdenite precipitation (Mathur et al., 2010; Greber et al., 2011; Shafiei et al., 2015; Yao et al., 2016). Therefore, the details of how Mo isotopes fractionate during fluid evolution and molybdenite precipitation are of interest.

We have shown that, for fine-grained molybdenite (0.2 mm, sample 1605-80/2-7), reproducible  $\delta^{98/95}\text{Mo}$  data were only obtained when the digested mass was greater than 5 mg, which contrasts with the coarse-grained molybdenite (2 mm, sample 1605-80/6-7), where reproducible  $\delta^{98/95}\text{Mo}$  data were obtained regardless of sample size. These two samples were obtained independently from a single molybdenite

vein and show no evidence of hydrothermal overprint, as evidenced by a homogeneous oxygen isotope composition of hydrothermal quartz grains associating these molybdenites and identical alteration assemblages along the vein. In addition, no fluid inclusion assemblages recording fluid boiling are documented. For these reasons, variations in temperature, pressure, pH, fluid boiling, and fluid mixing are not plausible explanations to account for variable  $\delta^{98/95}\text{Mo}$  in the fine-grained sample on a local scale. A simple explanation could be that these molybdenite grains were crystallized from fluids with different  $\delta^{98/95}\text{Mo}$ . If this is the case, the fluid must be heterogeneous in terms of Mo isotope composition at small scales (i.e., <0.2 mm) and homogeneous at large scales (i.e., >2 mm). Reducing Mo from its most oxidized state (i.e.,  $\text{Mo}^{6+}$ ; Rempel et al., 2006) to  $\text{Mo}^{4+}$  facilitates isotope fractionation (Rayleigh fractionation) because isotopically light Mo preferentially enters into molybdenite (Tossell, 2005). Therefore, we propose that the heterogeneity of  $\delta^{98/95}\text{Mo}$  at local scales was generated by localized Rayleigh fractionation (Fig. 6). For example, once mineralization has been initiated, the crystallization of molybdenite grains will fill the open spaces in fractures and prohibit sufficient convection and propagation of ore-forming fluid at small scales (i.e., <0.2 mm). For each localized system, the molybdenite grains that crystallize first will have lower  $\delta^{98/95}\text{Mo}$ , as regulated by Rayleigh fractionation (Fig. 7A). This process implies that the fluid was homogeneous in terms of  $\delta^{98/95}\text{Mo}$  prior to mineralization; thus, the development of localized Rayleigh fractionation throughout the system affects  $\delta^{98/95}\text{Mo}$  at the millimeter scale but does not create heterogeneous  $\delta^{98/95}\text{Mo}$  at larger scales. This hypothesis is supported by the homogeneous Mo isotope composition along single molybdenite veins once sufficient molybdenite was analyzed (Fig. 3C-E). We recommend that, for future studies, sufficient (e.g., >10 mg) molybdenite should be analyzed to overcome heterogeneity at the centimeter scale and to yield representative Mo isotope data.

#### *Hydrothermal controls on Mo isotope fractionation through time*

Now we turn to assessing the factors controlling  $\delta^{98/95}\text{Mo}$  under the framework of time-resolved fluid evolution. The predominant magmatic source of metals in porphyry deposits (Kouzmanov and Pokrovski, 2012; Cooke et al., 2014) makes the involvement of meteoric water (Fig. 4B) from a mass balance standpoint insignificant in terms of changing the Mo isotope composition of the fluid, and it is not discussed further. A lack of dependence between  $\delta^{98/95}\text{Mo}$  and temperature (Fig. 4A) precludes temperature as a dominant factor governing Mo isotope fractionation. Thus, the most likely candidates for generating the time-resolved  $\delta^{98/95}\text{Mo}$  patterns in Figure 5 are Rayleigh fractionation and/or fluid boiling. During the propagation of metalliferous fluid, as predicted by Rayleigh fractionation, successive crystallization of molybdenite from that fluid will generate progressively heavier  $\delta^{98/95}\text{Mo}$  (Fig. 7B; Greber et al., 2014). Consequently, this mechanism can explain the trend of increasing  $\delta^{98/95}\text{Mo}$  over time that is observed during the second mineralization pulse at Qulong (Fig. 5), with the exception of two veins that host higher  $\delta^{98/95}\text{Mo}$  (see below

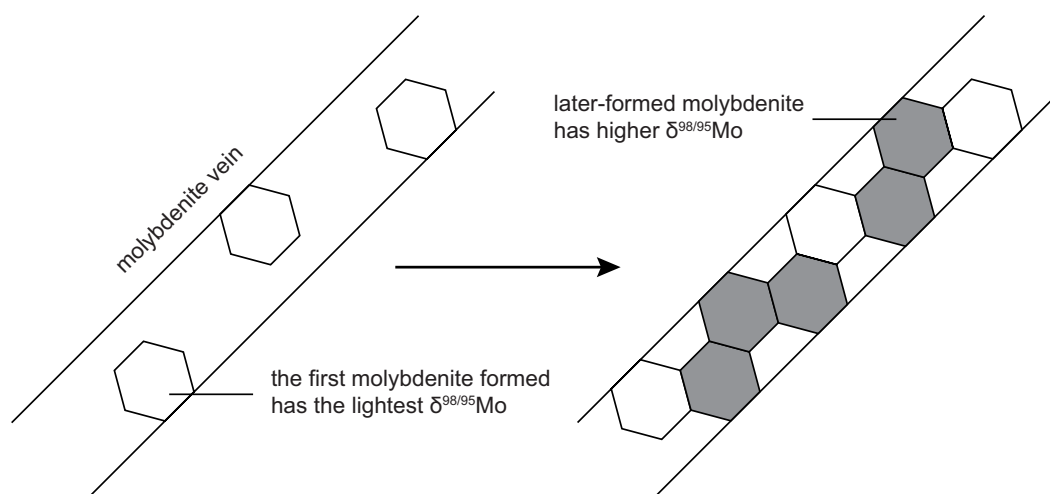


Fig. 6. Sketch illustrates that the heterogeneous Mo isotope composition at grain scale was controlled by Rayleigh fractionation. For fractures occupied by ore-forming fluid with a given  $\delta^{98/95}\text{Mo}$ , molybdenite grains that crystallized first will have the lightest  $\delta^{98/95}\text{Mo}$ , while molybdenite grains that crystallized later will have heavier  $\delta^{98/95}\text{Mo}$ . Without sufficient circulation of the ore-forming fluid during the short timescale of sulfide precipitation, the lighter  $\delta^{98/95}\text{Mo}$  signature will be preserved and give rise to heterogeneous  $\delta^{98/95}\text{Mo}$  at centimeter scale, whereas on a large scale  $\delta^{98/95}\text{Mo}$  becomes homogeneous.

for further discussion). However, the decreasing and invariable  $\delta^{98/95}\text{Mo}$  values in the first and third mineralization pulses (Fig. 5), respectively, require additional explanations.

Decompression-induced boiling also facilitates Mo isotope fractionation, and isotopically heavy Mo will preferentially enter the vapor phase over the liquid phase (Yao et al., 2016). Molybdenum is usually withheld in the liquid phase during boiling (Zajacz et al., 2017), and the vapor phase tends to rise above the porphyry-style mineralization site. As such, it is reasonable to assume that molybdenite in porphyry deposits predominantly precipitates from liquid phase after boiling.

In this regard, for a fluid undergoing multiple episodes of boiling, with isotopically heavy Mo preferentially being transported to the shallow levels, the residual liquid will progressively show lighter  $\delta^{98/95}\text{Mo}$  (Fig. 7B). Molybdenite grains crystallized successively from this residual fluid are expected to have decreasing  $\delta^{98/95}\text{Mo}$  with time unless the Mo isotope fractionation factor between molybdenite and fluid increases significantly with time. In all of the mineralization pulses, the temperature decreases through time, albeit with minor temporal fluctuations (Li et al., 2017a): this results in a decreasing fractionation factor over time. Therefore, we suggest that

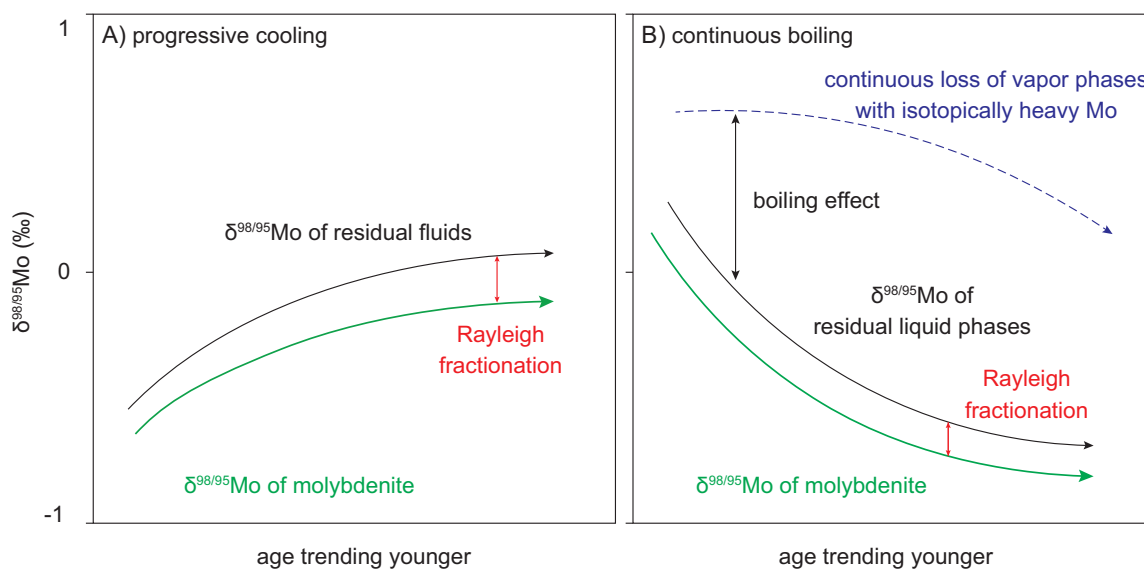


Fig. 7. Qualitative patterns of Mo isotope composition in an evolving system. A) For a system controlled by cooling, preferentially removing isotopically light Mo from the fluid to form molybdenite will make the residual fluid progressively isotopically heavier, and molybdenite grains will define a similar increasing  $\delta^{98/95}\text{Mo}$  trend below that of the residual fluid. B) For a system undergoing multiple episodes of fluid boiling, preferential enrichment of isotopically heavy Mo in the vapor phase will result in a progressive decrease in the  $\delta^{98/95}\text{Mo}$  pattern for the residual liquid phase. Molybdenite grains that precipitate from this liquid phase will have a similar decreasing  $\delta^{98/95}\text{Mo}$  trend.

successive boiling could generate decreasing  $\delta^{98/95}\text{Mo}$  with time similar to that documented at Kerman porphyry deposit, Iran (Shafiei et al., 2015), and observed in the first mineralization pulse here at Qulong (Fig. 5). The latter is partially supported by the presence of boiling fluid inclusion assemblages in the early-stage barren quartz veins (Li et al., 2017b). For the two veins that fall off the increasing trend in the second mineralization pulse (Fig. 5), the best explanation is that they were crystallized from vapor phases generated through intensive boiling (Fig. 7B). This is in accordance with the emplacement of the two-stage hydrothermal breccia (Yang et al., 2009; Li et al., 2017b). The ascent of the vapor phase with isotopically heavy Mo to shallow levels (Sillitoe, 2010; Zajacz et al., 2017) could result in the formation of molybdenite with heavier  $\delta^{98/95}\text{Mo}$  in the upper portion of a hydrothermal system (e.g., epithermal deposits). Interestingly, two molybdenite samples from the Freiberg district, Germany, which is an epithermal deposit, have elevated  $\delta^{98/95}\text{Mo}$  of 0.54 to 0.82‰ (Mathur et al., 2010) as predicted here.

From a mass balance perspective, generating significant Mo isotope fractionation through fluid boiling and Rayleigh fractionation requires a sufficient mass of Mo to be redistributed between the two phases involved (i.e., liquid vs. vapor in boiling; molybdenite vs. aqueous fluid in Rayleigh fractionation). For example, at 425° to 280°C, with a mineralization efficiency of ~10%, Rayleigh fractionation only generates molybdenites with a variation of ~0.069‰ in  $\delta^{98/95}\text{Mo}$  (Fig. 8), which is comparable to the current analytical precision and thus negligible. In addition, the degree of Mo isotope fractionation is also controlled by temperature (Fig. 8) and, at high temperature, less fractionation is expected in comparison to that at low temperature. The progressive cooling history at

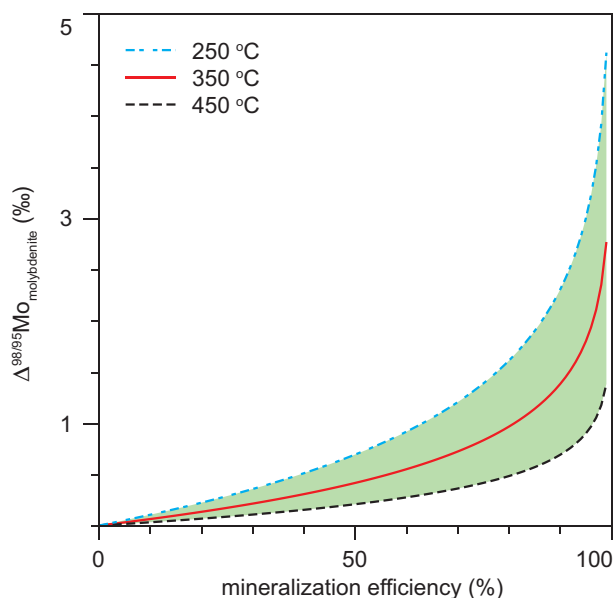


Fig. 8. Maximum molybdenum isotope variations of molybdenite ( $\Delta^{98/95}\text{Mo}_{\text{molybdenite}}$ ) that could be generated as a function of mineralization efficiency and temperature. For a given fluid,  $\delta^{98/95}\text{Mo}$  of molybdenite grains crystallized from that fluid could be predicted using a simple Rayleigh fractionation model, hence the  $\Delta^{98/95}\text{Mo}_{\text{molybdenite}}$ . The fractionation factors between molybdenite and fluid are assumed as 0.9990, 0.9994, and 0.9997 at 250°, 350°, and 450°C, respectively.

Qulong, though with fluctuations (Li et al., 2017a), suggests that temperature is unlikely a primary control for the variable degrees of Mo isotope fractionation for the three mineralization pulses. For these reasons, the significant Mo isotope fractionation observed in the first and second mineralization pulses implies intensive boiling and a high mineralization efficiency, respectively, while low mineralization efficiency could explain the lack of significant fractionation during the third mineralization pulse. This statement is supported by the progressive decrease (~60–<10%) in mineralization potential through time, which was constrained by an oxygen isotope study (Li et al., 2018).

#### *A mineralization efficiency perspective on Mo cycling*

During fluid boiling, isotopically heavy Mo is preferentially enriched in the vapor phase and then rises above the porphyry-style mineralization region due to its low density (Zajacz et al., 2017). Therefore, after fluid boiling, the liquid phase bearing isotopically light Mo is the predominant source of Mo for porphyry deposits. In addition, the crystallization of molybdenite favors isotopically light Mo, as predicted by Rayleigh fractionation. For these reasons, molybdenites from porphyry deposits are expected to have lighter  $\delta^{98/95}\text{Mo}$  in comparison to the initial ore-forming fluids. More importantly, the degree of enrichment in isotopically light Mo in porphyry deposits is largely controlled by mineralization efficiency (Fig. 7C). Although it has not been precisely constrained, mineralization efficiency rarely reaches 100%; hence, there must be a residual fluid hosting this isotopically heavy Mo after the formation of porphyry deposits. Interestingly, high-temperature hydrothermal systems with elevated  $\delta^{98/95}\text{Mo}$  (0–1.81‰) have been documented recently in Iceland (Neely et al., 2018), although molybdenite has not yet been reported.

Molybdenite and the residual fluid are expected to have contrasting recycling paths. For example, the residual fluid could either be trapped by phyllic and hypogene argillic alteration halos surrounding porphyry deposits or feed the surface hydrological system and eventually enter the oceans. Since hydrothermal alteration assemblages extend much farther than orebodies, this heavier  $\delta^{98/95}\text{Mo}$  inventory could be used as an efficient proxy to locate the mineralization center. For instance,  $\delta^{98/95}\text{Mo}$  values are expected to decrease from ore-barren alteration regions to an area that is well mineralized (i.e., molybdenite preferentially incorporates light Mo isotopes, producing lower  $\delta^{98/95}\text{Mo}$  toward the orebody). Similarly, significant isotope fractionations of Fe, Cu, and Zn are observed during ore-forming processes (Graham et al., 2004; Li et al., 2010; Zhu et al., 2018), and we suggest that their isotopic compositions could also have implications in mineral exploration.

Additionally, it is well established that porphyry deposits are unevenly distributed both in space and time (Richards, 2011). With porphyry deposits being predominately formed at convergent margins during certain periods in the geologic past (e.g., Miocene, Cretaceous), the ore-bearing margins of these continents could have a lighter  $\delta^{98/95}\text{Mo}$ , and a flux of residual fluid with heavier  $\delta^{98/95}\text{Mo}$  into the oceans may lead to a temporal increase in Mo isotope composition of the oceans. Such a spatial and temporal fluctuation in continental and marine  $\delta^{98/95}\text{Mo}$ , if sufficiently large, needs to be considered when

quantifying  $\delta^{98/95}\text{Mo}$  of the upper continental crust, constraining Mo cycling, and using  $\delta^{98/95}\text{Mo}$  of marine sediments as a paleoredox proxy. An in-depth investigation of the fate of this isotopically heavy residual fluid would require mass balance calculations and numerical modeling, which is beyond the scope of this study but should be considered in future studies.

### Conclusions

Decompression and cooling are inevitable outcomes of deep-sourced metalliferous magmatic fluids reaching conditions typical of porphyry-style mineralization (i.e., 1–3 km, 300°–450°C). These temperature-pressure conditions occur where water-rich fluid makes the transition from a supercritical fluid state to liquid and vapor phases and impact Mo isotope fractionation during ore formation. The short timescales of ore formation and the inefficiency of conductive cooling lead us to propose that the rapid cooling needed for efficient mineralization is facilitated by mixing hot magmatic fluid with cold meteoric water. We have demonstrated that the homogeneity of  $\delta^{98/95}\text{Mo}$  within single molybdenite veins and the heterogeneous  $\delta^{98/95}\text{Mo}$  within samples were regulated by Rayleigh fractionation. The  $\delta^{98/95}\text{Mo}$  of molybdenite during fluid evolution at Qulong was controlled by three separate processes: boiling, Rayleigh fractionation, and mineralization efficiency. If the fluid underwent multiple episodes of intensive boiling, lighter  $\delta^{98/95}\text{Mo}$  will develop over time. Rayleigh fractionation-dominated systems will show a heavier  $\delta^{98/95}\text{Mo}$ , and the  $\delta^{98/95}\text{Mo}$  will basically be invariant with low mineralization efficiency.

The preferential loss of isotopically heavy Mo through fluid boiling, the favorable incorporation of isotopically light Mo in molybdenite, and the fact that mineralization efficiency rarely reaches 100% together imply the presence of a residual fluid with heavier  $\delta^{98/95}\text{Mo}$ . This residual fluid could be recorded by alteration halos surrounding porphyry deposits; hence, the Mo (and potentially Fe, Cu, and Zn) isotope composition of alteration assemblages could potentially be utilized as a proxy to locate the mineralization center. Finally, due to the heterogeneous distribution of porphyry deposits in space and time, variations in mineralization efficiency and the presence of residual fluids enriched in heavy  $\delta^{98/95}\text{Mo}$  should be considered in future studies addressing elemental cycling.

### Acknowledgments

This work is supported by the Chinese Academy of Sciences Pioneer Hundred Talents Program and a grant (SKL-K201706) from the State Key Laboratory of Lithospheric Evolution. We thank Geoff Nowell for his laboratory support. DS acknowledges the Total Endowment Fund and the Dida Scholarship of CUG Wuhan. Constructive comments and suggestions from the editors and reviewers significantly improved the presentation of this paper.

### REFERENCES

- Breillat, N., Guerrot, C., Marcoux, E., and Négrel, P., 2016, A new global database of  $\delta^{98}\text{Mo}$  in molybdenites: A literature review and new data: *Journal of Geochemical Exploration*, v. 161, p. 1–15.
- Buret, Y., von Quadt, A., Heinrich, C., Selby, D., Walle, M., and Peytcheva, I., 2016, From a long-lived upper-crustal magma chamber to rapid porphyry copper emplacement: Reading the geochemistry of zircon crystals at Bajo de la Alumbrera (NW Argentina): *Earth and Planetary Science Letters*, v. 450, p. 120–131.
- Chelle-Michou, C., Rottier, B., Caricchi, L., and Simpson, G., 2017, Tempo of magma degassing and the genesis of porphyry copper deposits: *Scientific Reports*, v. 7, p. 40,566.
- Chiaradia, M., and Caricchi, L., 2017, Stochastic modelling of deep magmatic controls on porphyry copper deposit endowment: *Scientific Reports*, v. 7, p. 44,523.
- Cooke, D.R., Hollings, P., Wilkinson, J.J., and Tosdal, R.M., 2014, 13.14—Geochemistry of porphyry deposits, *in* Turekian, H.D.H.K., ed., *Treatise on geochemistry* (second edition): Oxford, Elsevier, p. 357–381.
- Creech, J.B., and Paul, B., 2015, IsoSpike: Improved double-spike inversion software: *Geostandards and Geoanalytical Research*, v. 39, p. 7–15.
- Dickson, A.J., 2017, A molybdenum-isotope perspective on Phanerozoic deoxygenation events: *Nature Geoscience*, v. 10, p. 721–726.
- Driesner, T., and Heinrich, C.A., 2007, The system  $\text{H}_2\text{O-NaCl}$ . Part I: Correlation formulae for phase relations in temperature-pressure-composition space from 0 to 1000°C, 0 to 5000bar, and 0 to 1 XNaCl: *Geochimica et Cosmochimica Acta*, v. 71, p. 4880–4901.
- Du, A.D., Wu, S.Q., Sun, D.Z., Wang, S.X., Qu, W.J., Markey, R., Stain, H., Morgan, J., and Malinovsky, D., 2004, Preparation and certification of Re-Os dating reference materials: Molybdenites HLP and JDC: *Geostandards and Geoanalytical Research*, v. 28, p. 41–52.
- Fekete, S., Weis, P., Driesner, T., Bouvier, A.S., Baumgartner, L., and Heinrich, C.A., 2016, Contrasting hydrological processes of meteoric water incursion during magmatic-hydrothermal ore deposition: An oxygen isotope study by ion microprobe: *Earth and Planetary Science Letters*, v. 451, p. 263–271.
- Goldberg, T., Gordon, G., Izon, G., Archer, C., Pearce, C.R., McManus, J., Anbar, A.D., and Rehkamper, M., 2013, Resolution of inter-laboratory discrepancies in Mo isotope data: An intercalibration: *Journal of Analytical Atomic Spectrometry*, v. 28, p. 724–735.
- Graham, S., Pearson, N., Jackson, S., Griffin, W., and O'Reilly, S.Y., 2004, Tracing Cu and Fe from source to porphyry: In situ determination of Cu and Fe isotope ratios in sulfides from the Grasberg Cu-Au deposit: *Chemical Geology*, v. 207, p. 147–169.
- Greber, N.D., Hofmann, B.A., Voegelin, A.R., Villa, I.M., and Nagler, T.F., 2011, Mo isotope composition in Mo-rich high- and low-T hydrothermal systems from the Swiss Alps: *Geochimica et Cosmochimica Acta*, v. 75, p. 6600–6609.
- Greber, N.D., Siebert, C., Nögler, T.F., and Pettke, T., 2012,  $\delta^{98/95}\text{Mo}$  values and molybdenum concentration data for NIST SRM 610, 612 and 3134: Towards a common protocol for reporting Mo data: *Geostandards and Geoanalytical Research*, v. 36, p. 291–300.
- Greber, N.D., Pettke, T., and Nagler, T.F., 2014, Magmatic-hydrothermal molybdenum isotope fractionation and its relevance to the igneous crustal signature: *Lithos*, v. 190, p. 104–110.
- Hannah, J.L., Stein, H.J., Wieser, M.E., de Laeter, J.R., and Varner, M.D., 2007, Molybdenum isotope variations in molybdenite: Vapor transport and Rayleigh fractionation of Mo: *Geology*, v. 35, p. 703–706.
- Hou, Z.Q., Yang, Z.M., Qu, X.M., Meng, X.J., Li, Z.Q., Beaudoin, G., Rui, Z.Y., Gao, Y.F., and Zaw, K., 2009, The Miocene Gangdese porphyry copper belt generated during post-collisional extension in the Tibetan orogen: *Ore Geology Reviews*, v. 36, p. 25–51.
- Hu, Y.B., Liu, J.Q., Ling, M.X., Ding, W., Liu, Y., Zartman, R.E., Ma, X.F., Liu, D.Y., Zhang, C.C., Sun, S.J., Zhang, L.P., Wu, K., and Sun, W.D., 2015, The formation of Qulong adakites and their relationship with porphyry copper deposit: Geochemical constraints: *Lithos*, v. 220, p. 60–80.
- Kendall, B., Dahl, T.W., and Anbar, A.D., 2017, Good golly, why moly? The stable isotope geochemistry of molybdenum: Non-Traditional Stable Isotopes, p. 82, p. 683–732.
- Kessel, R., Schmidt, M.W., Ulmer, P., and Pettke, T., 2005, Trace element signature of subduction-zone fluids, melts and supercritical liquids at 120–180 km depth: *Nature*, v. 437, p. 724–727.
- Klemm, L.M., Pettke, T., and Heinrich, C.A., 2008, Fluid and source magma evolution of the Questa porphyry Mo deposit, New Mexico, USA: *Mineralium Deposita*, v. 43, p. 533–552.
- Kouzmanov, K., and Pokrovski, G.S., 2012, Hydrothermal controls on metal distribution in porphyry Cu (-Mo-Au) systems: *Society of Economic Geologists, Special Publication 16*, p. 573–618.
- Landtwing, M.R., Pettke, T., Halter, W.E., Heinrich, C.A., Redmond, P.B., Einaudi, M.T., and Kunze, K., 2005, Copper deposition during quartz dissolution by cooling magmatic-hydrothermal fluids: The Bingham porphyry: *Earth and Planetary Science Letters*, v. 235, p. 229–243.

- Lawley, C.J.M., and Selby, D., 2012, Re-Os geochronology of quartz-enclosed ultrafine molybdenite: Implications for ore geochronology: *Economic Geology*, v. 107, p. 1499–1505.
- Li, W.Q., Jackson, S.E., Pearson, N.J., and Graham, S., 2010, Copper isotopic zonation in the Northparkes porphyry Cu-Au deposit, SE Australia: *Geochimica et Cosmochimica Acta*, v. 74, p. 4078–4096.
- Li, Y., Selby, D., Condon, D., and Tapster, S., 2017a, Cyclic magmatic-hydrothermal evolution in porphyry systems: High-precision U-Pb and Re-Os geochronology constraints on the Tibetan Qulong porphyry Cu-Mo deposit: *Economic Geology*, v. 112, p. 1419–1440.
- Li, Y., Selby, D., Feely, M., Costanzo, A., and Li, X.H., 2017b, Fluid inclusion characteristics and molybdenite Re-Os geochronology of the Qulong porphyry copper-molybdenum deposit, Tibet: *Mineralium Deposita*, v. 52, p. 137–158.
- Li, Y., Li, X.H., Selby, D., and Li, J.W., 2018, Pulsed magmatic fluid release for the formation of porphyry deposits: Tracing fluid evolution in absolute time from the Tibetan Qulong Cu-Mo deposit: *Geology*, v. 46, p. 7–10.
- Malinovsky, D., Rodushkin, I., Baxter, D.C., Ingri, J., and Ohlander, B., 2005, Molybdenum isotope ratio measurements on geological samples by MC-ICPMS: *International Journal of Mass Spectrometry*, v. 245, p. 94–107.
- Markey, R., Stein, H.J., Hannah, J.L., Zimmerman, A., Selby, D., and Creaser, R.A., 2007, Standardizing Re-Os geochronology: A new molybdenite reference material (Henderson, USA) and the stoichiometry of Os salts: *Chemical Geology*, v. 244, p. 74–87.
- Mathur, R., Brantley, S., Anbar, A., Munizaga, F., Maksae, V., Newberry, R., Vervoort, J., and Hart, G., 2010, Variation of Mo isotopes from molybdenite in high-temperature hydrothermal ore deposits: *Mineralium Deposita*, v. 45, p. 43–50.
- Mercer, C.N., Reed, M.H., and Mercer, C.M., 2015, Time scales of porphyry Cu deposit formation: Insights from titanium diffusion in quartz: *Economic Geology*, v. 110, p. 587–602.
- Neely, R.A., Gislason, S.R., Olafsson, M., McCoy-West, A.J., Pearce, C.R., and Burton, K.W., 2018, Molybdenum isotope behaviour in groundwaters and terrestrial hydrothermal systems, Iceland: *Earth and Planetary Science Letters*, v. 486, p. 108–118.
- Paton, C., Hellstrom, J., Paul, B., Woodhead, J., and Hergt, J., 2011, Iolite: Freeware for the visualisation and processing of mass spectrometric data: *Journal of Analytical Atomic Spectrometry*, v. 26, p. 2508–2518.
- Pearce, C.R., Cohen, A.S., and Parkinson, I.J., 2009, Quantitative separation of molybdenum and rhenium from geological materials for isotopic determination by MC-ICP-MS: *Geostandards and Geoanalytical Research*, v. 33, p. 219–229.
- Rempel, K.U., Migdisov, A.A., and Williams-Jones, A.E., 2006, The solubility and speciation of molybdenum in water vapour at elevated temperatures and pressures: Implications for ore genesis: *Geochimica et Cosmochimica Acta*, v. 70, p. 687–696.
- Richards, J.P., 2011, Magmatic to hydrothermal metal fluxes in convergent and collided margins: *Ore Geology Reviews*, v. 40, p. 1–26.
- Selby, D., and Creaser, R.A., 2001, Re-Os geochronology and systematics in molybdenite from the Endako porphyry molybdenum deposit, British Columbia, Canada: *Economic Geology*, v. 96, p. 197–204.
- Shafiei, B., Shamanian, G., Mathur, R., and Mirnejad, H., 2015, Mo isotope fractionation during hydrothermal evolution of porphyry Cu systems: *Mineralium Deposita*, v. 50, p. 281–291.
- Siebert, C., Nagler, T.F., and Kramers, J.D., 2001, Determination of molybdenum isotope fractionation by double-spike multicollector inductively coupled plasma mass spectrometry: *Geochemistry Geophysics Geosystems*, v. 2, 16 p., paper 2000GC000124.
- Sillitoe, R.H., 2010, Porphyry copper systems: *Economic Geology*, v. 105, p. 3–41.
- Spencer, E.T., Wilkinson, J.J., Creaser, R.A., and Seguel, J., 2015, The distribution and timing of molybdenite mineralization at the El Teniente Cu-Mo porphyry deposit, Chile: *Economic Geology*, v. 110, p. 387–421.
- Sun, W.D., Liang, H.Y., Ling, M.X., Zhan, M.Z., Ding, X., Zhang, H., Yang, X.Y., Li, Y.L., Ireland, T.R., Wei, Q.R., and Fan, W.M., 2013, The link between reduced porphyry copper deposits and oxidized magmas: *Geochimica et Cosmochimica Acta*, v. 103, p. 263–275.
- Tossell, J.A., 2005, Calculating the partitioning of the isotopes of Mo between oxidic and sulfidic species in aqueous solution: *Geochimica et Cosmochimica Acta*, v. 69, p. 2981–2993.
- Wang, R., Weinberg, R.F., Collins, W.J., Richards, J.P., and Zhu, D.C., 2018, Origin of postcollisional magmas and formation of porphyry Cu deposits in southern Tibet: *Earth-Science Reviews*, v. 181, p. 122–143.
- Weis, P., Driesner, T., and Heinrich, C.A., 2012, Porphyry-copper ore shells form at stable pressure-temperature fronts within dynamic fluid plumes: *Science*, v. 338, p. 1613–1616.
- Wilkinson, J.J., 2013, Triggers for the formation of porphyry ore deposits in magmatic arcs: *Nature Geoscience*, v. 6, p. 917–925.
- Willbold, M., and Elliott, T., 2017, Molybdenum isotope variations in magmatic rocks: *Chemical Geology*, v. 449, p. 253–268.
- Yang, J., Barling, J., Siebert, C., Fietzke, J., Stephens, E., and Halliday, A.N., 2017, The molybdenum isotopic compositions of I-, S- and A-type granitic suites: *Geochimica et Cosmochimica Acta*, v. 205, p. 168–186.
- Yang, Z.M., Hou, Z.Q., White, N.C., Chang, Z.S., Li, Z.Q., and Song, Y.C., 2009, Geology of the post-collisional porphyry copper-molybdenum deposit at Qulong, Tibet: *Ore Geology Reviews*, v. 36, p. 133–159.
- Yao, J.M., Mathur, R., Sun, W.D., Song, W.L., Chen, H.Y., Mutti, L., Xiang, X.K., and Luo, X.H., 2016, Fractionation of Cu and Mo isotopes caused by vapor-liquid partitioning, evidence from the Dahutang W-Cu-Mo ore field: *Geochemistry Geophysics Geosystems*, v. 17, p. 1725–1739.
- Zajacz, Z., Candela, P.A., and Piccoli, P.M., 2017, The partitioning of Cu, Au and Mo between liquid and vapor at magmatic temperatures and its implications for the genesis of magmatic-hydrothermal ore deposits: *Geochimica et Cosmochimica Acta*, v. 207, p. 81–101.
- Zhao, J.X., Qin, K.Z., Xiao, B., McInnes, B., Li, G.M., Evans, N., Cao, M.J., and Li, J.X., 2016a, Thermal history of the giant Qulong Cu-Mo deposit, Gangdese metallogenic belt, Tibet: Constraints on magmatic-hydrothermal evolution and exhumation: *Gondwana Research*, v. 36, p. 390–409.
- Zhao, P.P., Li, J., Zhang, L., Wang, Z.B., Kong, D.X., Ma, J.L., Wei, G.J., and Xu, J.F., 2016b, Molybdenum mass fractions and isotopic compositions of international geological reference materials: *Geostandards and Geoanalytical Research*, v. 40, p. 217–226.
- Zhu, Z.Y., Jiang, S.Y., Mathur, R., Cook, N.J., Yang, T., Wang, M., Ma, L., and Ciobanu, C.L., 2018, Iron isotope behavior during fluid/rock interaction in K-feldspar alteration zone—a model for pyrite in gold deposits from the Jiadong Peninsula, east China: *Geochimica et Cosmochimica Acta*, v. 222, supplement C, p. 94–116.



**Yang Li** is an associate professor at the Institute of Geology and Geophysics, Chinese Academy of Sciences. He received his B.Eng. and Ph.D. degrees from China University of Geosciences, Wuhan, and Durham University in 2011 and 2017, respectively, followed by postdoctoral training at Durham and Yale University. His current research broadly seeks to understand how metalliferous volatiles are concentrated in the upper crust and their fate near the surface through integrating field geology, high-precision geochronology, and isotopic microanalysis. Additional research interests include further developments and geologic applications of the Re-Os chronometer.